



The hydrothermal system of the Domuyo volcanic complex (Argentina): A conceptual model based on new geochemical and isotopic evidences



F. Tassi^{a,b,*}, C. Liccioli^c, M. Augusto^e, G. Chiodini^d, O. Vaselli^{a,b}, S. Calabrese^f, G. Pecoraino^g, L. Tempesti^a,
C. Caponi^a, J. Fiebig^h, S. Caliroⁱ, A. Caselli^c

^a Department of Earth Sciences, University of Florence, Via La Pira 4, 50121 Florence, Italy

^b CNR-IGG Institute of Geosciences and Earth Resources, Via La Pira 4, 50121 Florence, Italy

^c Instituto de Paleobiología y Geología de la Universidad Nacional Rio Negro, Rio Negro, Argentina

^d Istituto Nazionale di Geofisica e Vulcanologia, Via D. Creti 12, 40128 Bologna, Italy

^e Facultad de Ciencias Exactas y Naturales, Universidad de Buenos Aires, Buenos Aires, Argentina

^f Dipartimento di Scienze della Terra e del Mare, Università di Palermo, Palermo, Italy

^g Istituto Nazionale di Geofisica e Vulcanologia, Sezione di Palermo Via Ugo la Malfa 153, 90146 Palermo, Italy

^h Institut für Geowissenschaften, Goethe-Universität, Altenhöferallee 1, 60438 Frankfurt am Main, Germany

ⁱ Istituto Nazionale di Geofisica e Vulcanologia "Osservatorio Vesuviano", Via Diocleziano, Napoli 328-80124, Italy

ARTICLE INFO

Article history:

Received 8 April 2016

Received in revised form 28 October 2016

Accepted 2 November 2016

Available online 5 November 2016

Keywords:

Geothermal system

Hydrothermal fluid

Geothermometry

Domuyo volcanic complex

Alternative energy source

ABSTRACT

The Domuyo volcanic complex (Neuquén Province, Argentina) hosts one of the most promising geothermal systems of Patagonia, giving rise to thermal manifestations discharging hot and Cl^- -rich fluids. This study reports a complete geochemical dataset of gas and water samples collected in three years (2013, 2014 and 2015) from the main fluid discharges of this area. The chemical and isotopic composition ($\delta\text{D-H}_2\text{O}$ and $\delta^{18}\text{O-H}_2\text{O}$) of waters indicates that rainwater and snow melting are the primary recharge of a hydrothermal reservoir located at relative shallow depth (400–600 m) possibly connected to a second deeper (2–3 km) reservoir. Reactive magmatic gases are completely scrubbed by the hydrothermal aquifer(s), whereas interaction of meteoric waters at the surface causes a significant air contamination and dilution of the fluid discharges located along the creeks at the foothill of the Cerro Domuyo edifice. Thermal discharges located at relatively high altitude (~3150 m a.s.l.), namely Bramadora, are less affected by this process, as also shown by their relatively high R/Ra values (up to 6.91) pointing to the occurrence of an actively degassing magma batch located at an unknown depth. Gas and solute geothermometry suggests equilibrium temperatures up to 220–240 °C likely referred to the shallower hydrothermal reservoir. These results, confirming the promising indications of the preliminary surveys carried out in the 1980's, provide useful information for a reliable estimation of the geothermal potential of this extinct volcanic system, although a detailed geophysical measurements is required for the correct estimation of depth and dimensions of the fluid reservoir(s).

© 2016 Elsevier B.V. All rights reserved.

1. Introduction

Preliminary geophysical and geochemical investigations carried out at the Domuyo volcanic complex by a Japan–Argentine joint agency in 1983 and 1984 (JICA, 1983, 1984), at the northern edge of the Cordillera del Viento chain in the Neuquén Province (Argentina), recognized a promising geothermal resource related to the possible occurrence of two hydrothermal aquifers located at ≤ 600 and 2000–3000 m depth. The exploration of this system was interrupted at the feasibility phase, mainly due to its remote location, i.e. far from the main electricity supplies, and the creation of a provincial natural park. Hence, the energy

supply for the local communities currently consists of fossil fuels from the oil and gas fields in the neighboring Neuquén Basin, which have a high cost due to the lack of pipelines connecting this area with the production zones (Mas and Mas, 2015). In 2015, a renewed interest for geothermal resources caused by the economic crisis convinced the national government to financially support scientific projects aimed at investigating in more detail the Domuyo hydrothermal system. A recent study (Chiodini et al., 2014) carried out a preliminary evaluation of the thermal energy released from this system (~1 GW), based on the flux of Cl^- -rich fluids discharged from the thermal springs emerging in the western-slope of the volcanic edifice. These results highlighted the enormous geothermal potential of Domuyo, encouraging further investigations.

This paper describes and discusses the first complete dataset of chemical and isotopic composition of gas and waters samples collected

* Corresponding author at: Department of Earth Sciences, University of Florence, Via La Pira 4, 50121 Florence, Italy.

E-mail address: franco.tassi@unifi.it (F. Tassi).

from this area in 2013, 2014 and 2015. The main aims are to (i) investigate the origin of the thermal fluids and (ii) construct a geochemical conceptual model able to describe the chemical-physical characteristics of the hydrothermal reservoir and the fluid circulation patterns.

2. Regional setting and previous geothermal prospection

Domuyo (36°34'S, 70°25'W) is a volcanic complex emplaced from the Middle Miocene to Pleistocene in the Southern Volcanic Zone (SVZ), where volcanism is controlled by the subduction of the oceanic Nazca Plate below the continental lithosphere of the western side of South America (Farías et al., 2010). The total volume and the basal area of this volcanic system are ~200 km³ and 138 km², respectively (Völker et al., 2011), whereas the maximum altitude of the highest peak (Cerro Domuyo), known as the “Patagonian roof”, is 4709 m a.s.l. Domuyo belongs to a series of silicic calderas produced by a delamination process active underneath the thickest part of the Southern Andes in the last 1 My. It is hosted within extensional basins that crosscut the chain at latitudes between 35° and 39°S (Ramos et al., 2004). Cerro Domuyo (2.5 ± 0.5 My) is a wide rhyolitic dome unconformably emplaced in a N-S oriented anticline (Groeber, 1947; Llambías et al., 1978; Miranda et al., 2006; Folguera et al., 2007). Younger domes (720–110 ky) extruded according to a sub-circular geometry in the southwestern sector of Cerro Domuyo, whereas a minor intrusive body, generated by the last magmatic pulse in the Late Pleistocene (Miranda et al., 2006), occurs in the southern flank. Acidic rocks constituting the volcanic basement belong to the Choiyoi Group, a widely extended magmatic zone (~500,000 km² between 28° and 38°S) developed along the collision zone of the Patagonia allochthonous terrains against the proto-Gondwana during the Lower Permian (e.g. Kay et al., 1989, 2006; Kay and Abbruzzi, 1996). According to seismic reflection data, a hydrothermal reservoir is presumably hosted at 2–3 km depth in vertical structures, as pipes and “plate” fractures or faults, within the basement (JICA, 1984). The overlying Mesozoic formations consist of both deep (black shales) and shallow marine deposits, the latter including evaporitic carbonate and gypsum (Palma et al., 2012; Kietzmann and Vennari, 2013). Volcanic products intercalated with the sedimentary formations (Llambías and Leanza, 2005) are likely characterized by a relatively high permeability to circulating fluids (JICA, 1984). The Late Pliocene to Pleistocene volcanic rock sequences mainly consisting of rhyolitic lavas and associated phreatomagmatic products (Llambías et al., 1978), where geoelectrical and gravimetric measurements indicated the occurrence of a low resistivity (2–15 Ω m⁻¹) zone, are supposed to host the shallower hydrothermal aquifer (JICA, 1983, 1984). Tertiary and Quaternary welded tuffs and andesites, with a thickness ranging from 20 to 200 m, act as cap-rock. The tectonic setting is dominated by N-S- and E-W-oriented fault systems, the former being consistent with the direction of the main anticline into which the Cerro Domuyo intruded. Secondary NW- and NE-oriented fault systems were also recognized (JICA, 1984).

Palacio and Llambías (1978) provided the first, pioneering information about Domuyo fluid discharges. During the 1983–1984 prospection, twelve exploration wells were drilled down to 100 m depth in an area of 40 km² (JICA, 1983, 1984), which roughly corresponds to that investigated in the present study (Fig. 1). The maximum measured temperatures at the bottom of wells did not exceed ~90 °C.

3. Sampling and analytical methods

3.1. Water and gas sampling

Most hydrothermal discharges, consisting of fumaroles and bubbling and boiling pools, occur along creeks at the foothills (1740–2200 m a.s.l.) of Cerro Domuyo (Fig. 1), suggesting that the local tectonic setting strictly controls both the emergence of thermal fluids and the surface hydrological network. Noteworthy, in 2003, at the Humazo emission

(D1; Fig. 1), a site that was considered the most promising exploitation zone by JICA (1983, 1984), a phreatic explosion occurred, giving rise to a 300 m high plume and displacing blocks up to 1 ton (Mas et al., 2009). However, the most remarkable fluid emissions (D5; Fig. 1), known as Bramadora (*bramar* in Spanish means “to roar”) and discharging an ~15 m high vapor column, is located at ~3150 m a.s.l., SW of Cerro Domuyo (Fig. 1).

In the present study, 14 thermal water samples (T > 20 °C), from 11 different sites (D1–D11; Fig. 1), and 6 cold water samples (D12–D17; Fig. 1) from the Varvarco river and its tributaries, were collected. Temperature and pH were measured in situ with portable instruments (uncertainties: ± 0.1 °C and ± 0.05, respectively). Lab analyses were carried out for the determination of: i) chemical composition, ii) δD and δ¹⁸D values of water, and iii) δ¹³C ratios of total dissolved inorganic Carbon (TDIC). Water samples for the analysis of the anions were collected in 100 mL sterile polyethylene bottles, after filtering at 0.45 μm, whereas filtered and acidified (by adding Suprapur hydrochloric acid, HCl 1%) samples collected in 50 mL bottles were used for the analysis of the cations. The δD and δ¹⁸D values of water were analyzed on samples collected in 100 mL dark glass bottles, whereas the δ¹³C-TDIC values were determined in samples collected in 1000 mL glass bottles after the addition of SrCl₂ and NaOH to precipitate dissolved C as SrCO₃.

22 gas samples from 12 fumarolic vents were collected using a sampling line consisting of a 1 m long titanium tube (Ø = 2.5 cm) inserted into the fumarolic vent and connected to glass-dewared tubes. Bubbling gases (samples D9a and D9b; Fig. 1) were sampled using a plastic funnel, submerged upside-down in the pools, and tygon tubes connections. Both the fumaroles and bubbling gases were collected in pre-evacuated 60-mL glass thion-tapped flasks filled with 20 mL of a 4 N NaOH and 0.15 M Cd(OH)₂ suspension (Montegrossi et al., 2001; Vaselli et al., 2006). During sampling, water vapor and CO₂ dissolved in the alkaline solution, H₂S formed insoluble CdS, whereas low-solubility gas species (N₂, O₂, CO, H₂, He, Ar, CH₄ and light hydrocarbons) were trapped and stored in the flask head-space. Steam condensates (for the analysis of the δD and δ¹⁸D values of water) and dry gases (for the analysis of CO, ³He/⁴He and the ¹³C/¹²C ratio in CO₂) were sampled from the fumaroles using a water-cooled condenser connected to the sampling line adopted for the soda flasks. In 2013 at the D1, D2, D3 and D9 fumaroles and in 2014 at the D5 site, an additional gas sample was collected in 100 mL sampling glass flasks filled with 50 mL of a 4 N NaOH solution for the analysis of the δ¹⁵N value in N₂ and the ⁴⁰Ar/³⁶Ar.

The UTM coordinates (WGS 84 Zone 19H) of the water and gas sampling sites are reported in Table 1 and plotted in Fig. 1.

3.2. Chemical and isotopic analysis of waters

Major cations (Na⁺, K⁺, Ca²⁺, Mg²⁺, Li⁺ and NH₄⁺) and anions (F⁻, Cl⁻, SO₄²⁻, Br⁻ and NO₃⁻) were analyzed at the Department of Earth Sciences of Florence (Italy) by ion chromatography (IC) using a Metrohm 861 and Metrohm 761, respectively. Total alkalinity (HCO₃⁻ and CO₃²⁻) was determined by acidimetric titration (AT) with HCl 0.5 N using a Metrohm 794 Basic Titrino. Boron was analyzed using the Azomethine-H method (Bencini, 1985) by molecular spectrophotometry (MS; Philips Unicam SP6-350). The latter instrument was also used for the analysis of SiO₂. The analytical errors for AT, IC and MS analyses were ≤ 5%. In water samples collected in 2013 and 2014, the analysis of the carbon (δ¹³C-TDIC), oxygen (δ¹⁸O-H₂O), after equilibration with CO₂-H₂O (Epstein and Mayeda, 1953), and hydrogen (δD-H₂O), obtained after the reaction of 10 μL of water with metallic zinc at 500 °C (Coleman et al., 1982), isotopic values were carried out at the Geochemistry Laboratory of INGV-Osservatorio Vesuviano (Naples, Italy). A Finnigan Delta plusXP continuous flow mass spectrometer was used in combination with a GasbenchII device. The analytical errors were: δD-H₂O ± 1‰, δ¹⁸O-H₂O ± 0.08‰ and δ¹³C-TDIC ± 0.06‰. The δ¹⁸O-H₂O and δD-H₂O value of waters and gas condensates collected in 2015 were determined at the Department of Physics and Earth

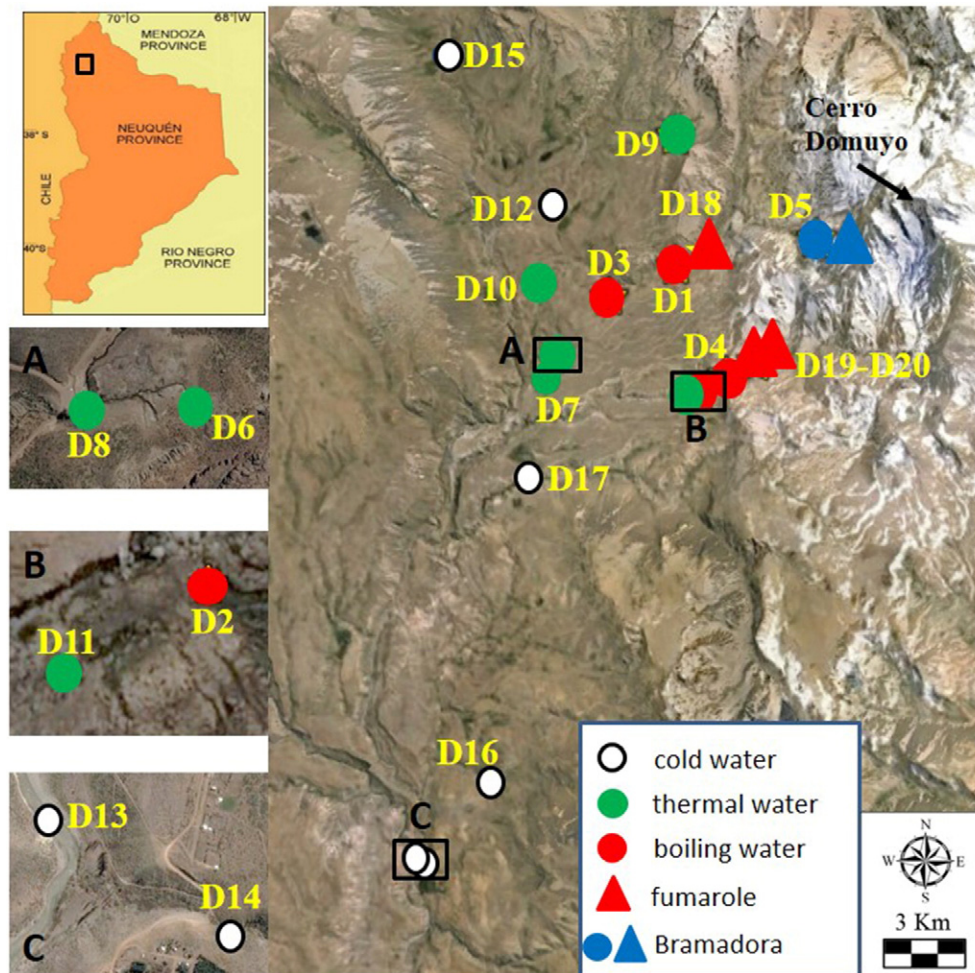


Fig. 1. Satellite image (Google Earth) of the study area with the location of the sampling sites. White circle: cold water ($T < 20\text{ }^{\circ}\text{C}$); green circle: thermal water ($T < 70\text{ }^{\circ}\text{C}$); red circle: thermal water ($T > 90\text{ }^{\circ}\text{C}$); red up triangle: fumarole; blue circle: Bramadora thermal water; blue up triangle: Bramadora fumarole.

Science (University of Parma, Italy) using a Thermo-Finnigan HDO equilibrator coupled to a mass spectrometer with double entry system Thermo-Finnigan Delta Plus. The analytical errors were $\pm 0.05\%$ and $\pm 1\%$ for $\delta^{18}\text{O-H}_2\text{O}$ and $\delta\text{D-H}_2\text{O}$, respectively.

3.3. Chemical and isotopic analysis of gases

The chemical composition of gases was determined at the Department of Earth Sciences of the University of Florence (Italy). Inorganic gases (N_2 , $\text{Ar} + \text{O}_2$, H_2 , He and CO) in the flask headspace were analyzed using a Shimadzu 15A gas chromatograph (GC) equipped with a 10 m long 5A molecular sieve column and a thermal conductivity detector (TCD). Argon and O_2 were analyzed using a Thermo Focus gas chromatograph equipped with a 30 m long capillary molecular sieve column and a TCD. A Shimadzu 14A gas chromatograph (GC), equipped with a 10-m-long stainless steel column packed with Chromosorb PAW 80/100 mesh coated with 23% SP 1700 and a flame ionization detector (FID), was used to analyze CH_4 and light hydrocarbons. In the liquid phase, CO_2 (as CO_3^{2-}) and H_2S (as SO_4^{2-}) were analyzed by AT and IC, respectively. The analytical errors for GC analyses were $< 5\%$.

The analysis of $^{13}\text{C}/^{12}\text{C}$ of CO_2 (expressed as $\delta^{13}\text{C-CO}_2$ ‰ vs. V-PDB) was carried out at the CNR-IGG laboratories (Pisa, Italy) using a Finnigan Delta S mass spectrometer after standard extraction and purification procedures of the gas mixtures (Evans et al., 1998; Vaselli et al., 2006). Carrara and San Vincenzo marbles (Internal), as well as NBS18 and NBS19 (International) standards were used to estimate the

external precision. The analytical error was $\pm 0.05\%$ and $\pm 0.1\%$, respectively. The He isotopic ratios (expressed as R/R_a , where R is the $^3\text{He}/^4\text{He}$ measured ratio and R_a is the $^3\text{He}/^4\text{He}$ ratio in the air: 1.39×10^{-6} ; Mamyryn and Tolstikhin, 1984) were determined at the INGV laboratories of Palermo (Italy). The gas mixture was purified in a stainless-steel preparation line in order to remove all species other than noble gases. He and Ne were cryogenically separated at 42 and 82 K, respectively. The $^3\text{He}/^4\text{He}$ ratio and ^{20}Ne content were analyzed by a Helix SFT-GVI mass spectrometer, following internal protocol (Rizzo et al., 2015). The analytical uncertainty in the determination of elemental He and Ne contents was $< 5\%$. Typical blanks for He and Ne were below 10^{-15} mol. The analytical error was $\leq 1\%$. The R/R_a values were corrected for atmospheric contamination using the $^4\text{He}/^{20}\text{Ne}$ ratios (Poreda and Craig, 1989), as follows:

$$R/R_a = [(R/R_a)_{\text{measured}} - r] / (1 - r) \quad (1)$$

where r is $(^4\text{He}/^{20}\text{Ne})_{\text{air}} / (^4\text{He}/^{20}\text{Ne})_{\text{measured}}$ [$(^4\text{He}/^{20}\text{Ne})_{\text{air}} = 0.318$; (Ozima and Posodek, 1983)].

The $\delta^{15}\text{N}$ in N_2 ($\delta^{15}\text{N-N}_2$ expressed as ‰ vs. air) and the $^{40}\text{Ar}/^{36}\text{Ar}$ ratios were determined at the INGV laboratories of Naples (Italy) using an Agilent 6890 N gas chromatograph (GC), equipped with a molecular sieve column and a TCD, coupled with a Finnigan Delta plusXP continuous-flow mass spectrometer (MS) equipped with a standard triple collector for the simultaneous determination of ^{36}Ar and ^{15}N . A post column switching device (Denswitch) allowed (i) to split the column

Table 1
Chemical and stable isotopic ($\delta^{18}\text{O}\text{-H}_2\text{O}$ and $\delta\text{D}\text{-H}_2\text{O}$, in ‰ vs. V-SMOW; $\delta^{13}\text{C}\text{-TDIC}$, in ‰ vs. V-PDB) composition of cold ($T < 20^\circ\text{C}$) and thermal ($T > 20^\circ\text{C}$) waters from the Domuyo volcanic complex. Concentrations are in mg/L. Geographic coordinates (UTM; WGS-84 195), altitude (m), and pH values, outlet temperature ($^\circ\text{C}$) and equilibrium temperature calculated using the SiO_2 (Fournier and Potter, 1982) and Na-K ($T_{\text{Na-K}}$; Giggienbach, 1988) geothermometers are also reported.

Name	Date	ID	Latitude	Longitude	Altitude	T	pH	HCO ₃ ⁻	CO ₃ ²⁻	F	Cl	Br	NO	SO ₂	Ca ²⁺	Mg ²⁺	Na	K	NH	Li	TDS	SiO ₂	B	$\delta^{13}\text{C}\text{-TDIC}$	$\delta^{18}\text{C}$	δD	T _{SiO2}	T _{Na-K}
El Humazo	2014	D1b	361,002	5,942,747	1991	97	8.32	124	0.06	4.6	1720	11	1.30	308	45	3.10	1160	141	4.0	11	3534	250	13	-12.9	-13.7	-114	181	249
El Humazo	2015	D1d	361,002	5,942,747	1991	92	8.05	122	6.2	6.2	2230	7.8	1.1	258	83	3.8	1380	160	1.8	14	4266	241	8.9	-11.9	-13.4	-111	179	245
Los Tachos	2014	D2b	361,901	5,938,273	2043	94	7.90	160	5.9	5.9	1780	6.0	0.86	230	57	1.9	1270	63	2.6	11	3588	241	11	-11.9	-13.4	-111	179	182
Los Tachos	2015	D2c	361,901	5,938,273	2043	93	8.54	110	5.3	5.3	1920	6.9	0.79	202	37	0.75	1200	77	3.1	10	3573	236	8.5	-13.0	-13.1	-110	168	188
Las Olletas	2014	D3b	358,400	5,941,715	1870	94	n.a.	464	4.0	4.0	1420	4.8	0.51	164	55	1.9	1100	60	2.4	9.8	3286	200	10	-13.0	-13.1	-110	168	188
Las Olletas	2015	D3c	358,400	5,941,715	1870	91	7.92	110	5.0	5.0	1680	6.1	0.69	170	43	0.20	1060	74	2.9	9.4	3161	196	6.5	-13.0	-13.1	-110	167	206
El Humazo De Los Tachos	2015	D4b	363,028	5,938,807	2170	92	8.56	98	6.4	6.4	2570	9.2	0.91	300	50	1.7	1600	160	2.3	15	4812	192	13	-13.1	-14.0	-112	177	214
Bramadora	2014	D5f	367,021	5,943,307	3144	96	7.00	372	0.53	0.53	168	0.38	0.37	57.6	199	5.5	38	21	2.57	0.51	865	218	0.4	-12.4	-14.0	-112	177	214
Agua Calientes vertiente	2014	D6	356,511	5,939,451	1762	67	6.72	134	2.6	2.6	930	2.9	0.87	119	27	1.60	630	50	1.4	5.5	1905	191	6.1	-12.1	-14.6	-114	166	204
Bagno La Piedra	2014	D7	356,044	5,938,722	1740	48	6.90	153	1.4	1.4	720	2.6	1.5	83	24	2.9	560	39	1.2	4.7	1593	161	3.2	-12.1	-14.6	-114	166	204
Agua Calientes salida	2014	D8	356,362	5,939,441	1739	46	7.83	166	2.4	2.4	920	3.8	0.86	112	40	2.8	705	46	1.3	6.0	2006	180	3.5	-9.58	-14.7	-115	173	201
Las Papas	2014	D9b	361,265	5,947,249	2196	40	6.07	1280	2.1	2.1	2330	10	0.80	126	271	56	1690	107	0.41	11	5884	123	4.6	-3.77	-14.0	-118	149	198
Manchana Covunco	2014	D10	355,626	5,942,334	1995	28	8.77	137	1.98	2.8	800	3.2	1.1	275	104	5.2	590	63	0.77	5.0	1989	121	5.4	-12.3	-14.3	-114	148	238
Covunco	2014	D11	361,863	5,938,249	2038	22	8.53	116	0.97	0.31	606	2.1	1.1	168	66	4.1	433	4.3	0.86	3.7	1406	136	4.7	-13.8	-14.2	-111		
Ailenco	2014	D12	356,191	5,945,057	1658	18	9.36	67	6.3	0.15	20	0.02	0.07	4.1	11	4.5	18	3.9	0.09	0.13	136	n.a.	n.a.	-7.36	-14.5	-111		
Varvarco Abajo	2014	D13	350,368	5,921,369	1184	16	n.a.	93	0.50	0.50	140	0.43	7.7	123	62	3.2	108	12	0.25	1.0	552	n.a.	n.a.	-10.1	-13.9	-106		
Arroyo Chagay	2014	D14	353,555	5,924,284	1474	16	6.86	49	0.14	0.14	0.60	n.d.	0.30	0.70	7.0	2.6	3.3	2.3	0.03	0.05	66	n.a.	n.a.	-13.8	-12.9	-100		
Varvarco	2014	D15	352,305	5,950,486	1581	16	8.57	90	0.82	0.27	4.3	n.d.	0.11	131	7.0	3.0	5.7	2.2	0.08	0.10	307	n.a.	n.a.	-8.60	-13.2	-101		
Arroyo Manzano	2014	D16	350,831	5,921,095	1252	14	7.03	95	0.29	0.29	3.0	n.d.	3.0	5.0	14	5.0	1.1	1.6	0.50	0.05	138	n.a.	n.a.	-15.0	-13.4	-103		
Atreuco	2014	D17	355,327	5,935,187	1668	11	7.64	15	0.27	0.27	4.3	n.d.	0.10	6.2	4.3	0.87	3.6	1.1	0.15	0.08	36	n.a.	n.a.	-9.21	-14.2	-107		

gas flow to the TCD and to the MS, and (ii) to invert the column flow after the species of interest (Ar and N₂) has reached the detector, preventing undesirable species (mainly CO and water) from reaching the MS. Analytical errors were: $\delta^{15}\text{N} \pm 0.1\text{‰}$, $^{36}\text{Ar} < 1\%$, $^{40}\text{Ar} < 3\%$.

The $^{13}\text{C}/^{12}\text{C}$ ratio of methane ($\delta^{13}\text{C}\text{-CH}_4$), ethane ($\delta^{13}\text{C}\text{-C}_2\text{H}_6$) and propane ($\delta^{13}\text{C}\text{-C}_3\text{H}_8$) in the G5a sample were carried out at the Institut für Geowissenschaften, Goethe University of Frankfurt (Germany), according to the method described in Fiebig et al. (2015). The hydrocarbons were transferred from the flask headspace to a pre-concentration system, consisting of two cryofocus devices packed with Porapak Q (50–80 mesh). Then, they passed through a GC column (GS CarbonPlot, Agilent) using He as gas carrier and oxidized to CO₂ at 940 °C using a NiO/CuO/Pt catalyst. The $^{13}\text{C}/^{12}\text{C}$ ratios of CO₂ produced, separately, from the 3 alkanes were analyzed by a MAT 253 mass spectrometer. External precision and reproducibility were $\pm 0.2\text{‰}$.

4. Results

4.1. Chemical and isotopic ($\delta^{18}\text{O}\text{-H}_2\text{O}$, $\delta\text{D}\text{-H}_2\text{O}$, $\delta^{13}\text{C}\text{-TDIC}$) composition of waters

The chemical and isotopic composition of the studied waters is reported in Table 1. Samples from the D1–D4 discharges, having outlet temperatures (from 91 to 97 °C) close to the boiling point at the discharge altitude (from 1870 to 3140 m a.s.l.), were characterized by relatively high pH (from 7.90 to 8.56), Total Dissolved Solids (TDS) values ranging from 865 to 4812 mg/L and a Na⁺-Cl⁻ composition (Fig. 2a,b). The D5f water sample, although characterized by a similar outlet temperature (96 °C), showed a Ca²⁺-HCO₃⁻ composition and lower pH (7.00) and TDS (865 mg/L). In all the high temperature waters, relatively high concentrations of SiO₂ (from 192 to 250 mg/L), B (up to 13 mg/L), Li⁺ (from 9.4 to 15 mg/L), NH₄⁺ (from 1.8 to 4 mg/L) and F⁻ (up to 6.4 mg/L) were also measured. The D12–D17 waters had T ≤ 18 °C, pH varying in a wide range (from 6.86 to 9.36), and relatively low TDS values (from 36 to 552 mg/L). Among them, the D12, D14, D16 and D17 samples showed a Ca²⁺-HCO₃⁻ composition, whereas D13 and D15 (Varvarco river) had Ca²⁺-SO₄²⁻ and Na⁺-Cl⁻ compositions, respectively (Fig. 2a,b). The concentrations of Li⁺, NH₄⁺ and F⁻ in all the cold waters were <1 mg/L. The D6, D7, D8, D10 and D11 waters, i.e. those characterized by outlet temperatures intermediate (from 22 to 67 °C) with respect to those of the previous two groups, showed a Na⁺-Cl⁻ composition (Fig. 2a,b), TDS from 1406 to 2006 mg/L and pH ranging from 6.72 to 8.77. The D9b sample (Las Papas), which is a Na⁺-Cl⁻, relatively stagnant bubbling pool with an outlet temperature of 40 °C, showed distinct chemical features being characterized by a weakly acidic pH (6.07) and the highest TDS value (5884 mg/L).

The $\delta^{18}\text{O}\text{-H}_2\text{O}$ and $\delta\text{D}\text{-H}_2\text{O}$ values (from -14.7‰ to -12.9‰ and from -118.4‰ to -100.5‰ vs. V-SMOW, respectively), as well as the $\delta^{13}\text{C}\text{-TDIC}$ values (from -15.0‰ to -3.7‰ vs. V-PDB), showed apparently no significant relationships with the other chemical-physical features.

4.2. Chemical and isotopic composition of gases

The outlet temperatures of the fumaroles ranged from 91 to 107 °C (Table 2). Their chemical composition (Table 2) was largely dominated by water vapor (from 979 to 996 mmol/mol), whereas dry gases mostly consisted of CO₂ (from 718 to 824 mmol/mol) and N₂ (from 75 to 216 mmol/mol). The concentrations of CH₄, H₂ and O₂ were varying in relatively wide intervals (from 0.78 to 91, from 0.12 to 105 and from 0.39 to 37 mmol/mol, respectively), whereas those of Ar and He were ≤5.2 and ≤0.19 mmol/mol, respectively. Among these gases, the Bramadora samples (D5a–e) can clearly be distinguished by their relatively high H₂, CH₄, H₂S and CO concentrations (up to 105, 95, 1.1 and 0.0071 mmol/mol, respectively) if compared to the other fumaroles (≤0.39, ≤5.9, ≤0.08 and <0.0005 mmol/mol, respectively). Light hydrocarbons in all

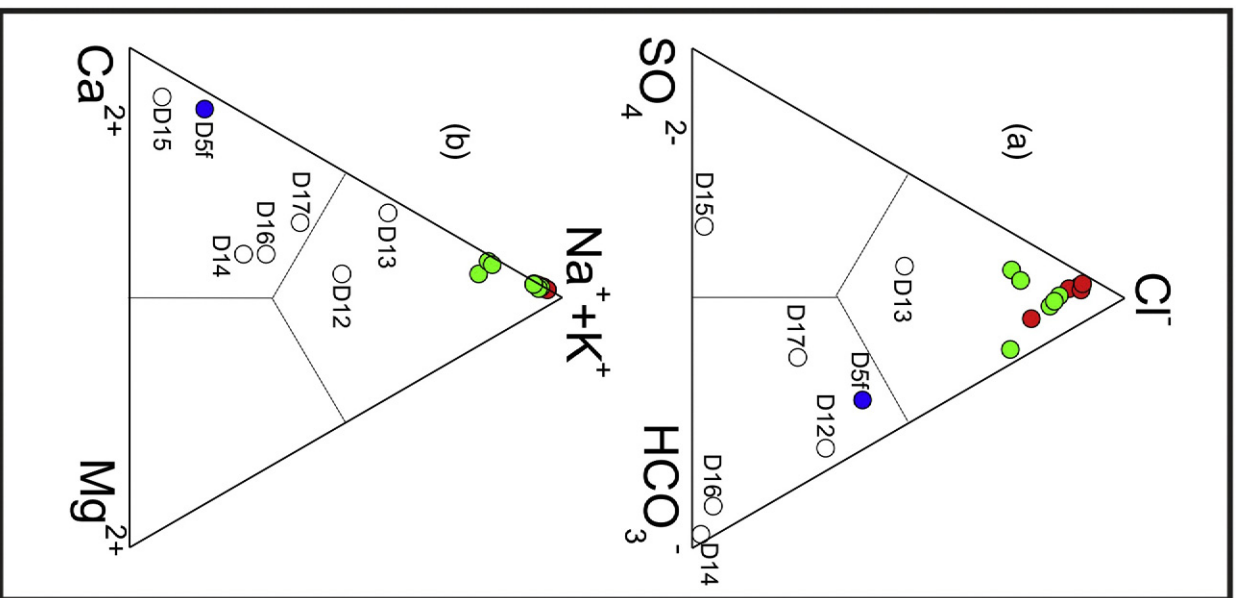


Fig. 2. (a) HCO_3^- - Cl^- - SO_4^{2-} and (b) Ca^{2+} - $(\text{Na}^+ + \text{K}^+)$ - Mg^{2+} ternary diagrams for cold and thermal waters from the Domuyo volcanic complex. Concentrations are in meq/L. Symbols as in Fig. 1.

the fumaroles consisted of ethane (C_2H_6 , from 0.021 to 0.12 mmol/mol), propane (C_3H_8 , from 0.0016 to 0.0091 mmol/mol), propene (C_3H_6 , from 0.0000022 to 0.000016 mmol/mol), benzene (C_6H_6 , from 0.0015 to 0.044 mmol/mol) and toluene (C_7H_8 , from 0.00011 to 0.0016 mmol/mol).

The two samples from the Las Papias bubbling pool (D9a,b) showed CO_2 and N_2 concentrations up to 949 and 45 mmol/mol, respectively. Oxygen, Ar and He concentrations were up to 11, 0.97 and 0.0018 mmol/mol, respectively, i.e. similar to those of fumarolic gases, whereas the abundances of H_2 and light hydrocarbons, including CH_4 , were 2–3 orders of magnitude lower. Carbon monoxide and H_2S were not detected.

The R/Ra values varied in a wide range, from 1.86 to 6.91, whereas the $\delta^{13}\text{C}$ - CO_2 values spanned in a narrow range, from -6.95% to -9.58% vs. V-PDB (Table 3). The $^{40}\text{Ar}/^{39}\text{Ar}$ values were almost identical to that of air (296), whereas the $\delta^{15}\text{N}_2$ values ranged from -3.1% to -0.1% vs. air. The only measured $\delta^{13}\text{C}$ - CH_4 value (D5a) was -29.6%

Table 2

Chemical composition of fumaroles and bubbling gases from the Domuyo volcanic complex. Concentrations are in mmol/mol. Geographic coordinates (UTM; WGS-84 19S), altitude (m) and outlet temperature ($^\circ\text{C}$) are also reported.

ID	Type	Latitude	Longitude	Altitude	T	CO_2	H_2S	N_2	CH_4	Ar	O_2	H_2	He	CO	C_2H_6	C_3H_8	C_3H_6	C_6H_6	C_7H_8	Water vapor
D1a	Fumarole	361,002	5,942,747	1991	98	781	0.08	178	1.6	3.9	35	0.34	0.0080	<0.0005	0.033	0.0047	0.00000024	0.0019	0.00013	993
D1b	Fumarole	361,002	5,942,747	1991	97	795	0.05	186	1.4	3.7	13	0.39	0.0067	<0.0005	0.045	0.0066	0.00000038	0.0021	0.00019	993
D1c	Fumarole	361,002	5,942,747	1991	97	824	0.06	155	5.9	3.4	11	0.31	0.0069	<0.0005	0.087	0.0091	0.00000065	0.0048	0.00025	991
D1d	fumarole	361,002	5,942,747	1991	92	813	0.04	169	3.6	3.7	10	0.25	0.0061	<0.0005	0.095	0.0087	0.00000079	0.0056	0.00026	992
D2a	Fumarole	361,901	5,938,273	2043	98	782	<0.01	186	2.4	4.1	25	0.14	0.081	<0.0005	0.054	0.0048	0.00000033	0.0024	0.00015	995
D2b	Fumarole	361,901	5,938,273	2043	94	775	<0.01	195	2.2	4.4	23	0.12	0.19	<0.0005	0.056	0.0066	0.00000038	0.0026	0.00018	994
D2c	Fumarole	361,901	5,938,273	2043	93	795	<0.01	177	2.6	3.9	21	0.13	0.086	<0.0005	0.061	0.0078	0.00000046	0.0036	0.00021	994
D3a	Fumarole	358,400	5,941,715	1870	97	764	>0.01	194	0.96	3.6	37	0.16	0.011	<0.0005	0.021	0.0035	0.00000022	0.0031	0.00014	996
D3b	Fumarole	358,400	5,941,715	1870	94	789	<0.01	175	0.78	4.2	31	0.13	0.0082	<0.0005	0.033	0.0026	0.00000025	0.0015	0.00015	994
D3c	Fumarole	358,400	5,941,715	1870	91	741	>0.01	216	1.1	5.2	36	0.26	0.0066	>0.0005	0.021	0.0031	0.00000026	0.0018	0.00011	993
D4a	Fumarole	363,028	5,938,807	2170	95	777	<0.01	191	1.2	4.2	26	0.24	0.023	<0.0005	0.051	0.0055	0.00000044	0.0023	0.00021	992
D4b	Fumarole	363,028	5,938,807	2170	92	794	<0.01	179	1.1	4.1	22	0.16	0.025	<0.0005	0.036	0.0041	0.00000032	0.0015	0.00013	993
D5a	Fumarole	367,021	5,943,307	3144	107	801	0.89	78	54	0.79	0.55	65	0.031	0.0038	0.087	0.0081	0.00000016	0.044	0.0012	979
D5b	Fumarole	367,021	5,943,307	3144	92	737	0.71	75	95	0.75	0.85	91	0.042	0.0041	0.11	0.0093	0.00000015	0.036	0.0016	987
D5c	Fumarole	367,021	5,943,307	3144	92	737	0.65	81	85	0.83	0.78	95	0.046	0.0045	0.12	0.0095	0.00000016	0.031	0.0011	986
D5d	Fumarole	367,021	5,943,307	3144	105	718	1.1	89	91	0.69	0.51	101	0.035	0.0066	0.096	0.0096	0.00000015	0.025	0.0014	981
D5e	Fumarole	367,021	5,943,307	3144	93	731	0.79	80	83	0.77	0.39	105	0.049	0.0071	0.087	0.0087	0.00000020	0.021	0.0015	985
D9a	Bubbling pool	361,265	5,947,249	2196	38	947	<0.01	41	0.014	0.93	11	0.0005	0.0012	<0.0005	0.00036	0.000055	<0.00000005	0.00022	0.000008	55
D9b	Bubbling pool	361,265	5,947,249	2196	40	949	<0.01	45	0.016	0.97	5.4	0.00042	0.0018	<0.0005	0.00031	0.000047	<0.00000005	0.00026	0.000009	41
D18	Fumarole	362,460	5,943,802	2256	94	806	0.07	172	1.3	4.2	16	0.21	0.0058	<0.0005	0.036	0.0028	0.00000045	0.0023	0.00019	994
D19	Fumarole	364,129	5,939,286	2308	95	816	0.04	156	2.4	3.5	22	0.41	0.0071	<0.0005	0.041	0.0053	0.00000041	0.0025	0.00017	992
D20	Fumarole	364,129	5,939,286	2308	91	822	0.07	144	2.0	3.3	28	0.36	0.0075	<0.0005	0.039	0.0044	0.00000037	0.0018	0.00016	984

Table 3

Stable isotopic ($\delta^{13}\text{C-CO}_2$ in ‰ vs. V-PDB; $\delta^{13}\text{C-CH}_4$, $\delta^{13}\text{C-C}_2\text{H}_6$ and $\delta^{13}\text{C-C}_3\text{H}_8$ in ‰ vs. V-PDB; $\delta^{18}\text{O-H}_2\text{O}_v$ and $\delta\text{D-H}_2\text{O}_v$ in ‰ vs. V-SMOW; $\delta^{15}\text{N}_2$ in ‰ vs. air; R/Ra; $^{40}\text{Ar}/^{36}\text{Ar}$) composition of fumaroles and bubbling gases from the Domuyo volcanic complex. $^4\text{He}/^{20}\text{Ne}$ and $\text{CO}_2/{}^3\text{He}$ ratios are also reported.

ID	R/Ra	$^{40}\text{Ar}/^{36}\text{Ar}$	$^4\text{He}/^{20}\text{Ne}$	$\delta^{13}\text{C-CO}_2$	$\delta^{18}\text{O-H}_2\text{O}_v$	$\delta\text{D-H}_2\text{O}_v$	$\delta^{15}\text{N}$	$\delta^{13}\text{C-CH}_4$	$\delta^{13}\text{C-C}_2\text{H}_6$	$\delta^{13}\text{C-C}_3\text{H}_8$	$\text{CO}_2/{}^3\text{He} \times 10^9$
D1a	1.92	295	1.3	-7.05			-3.1				36.6
D1b	1.86		1.5								45.9
D1d	1.95		2.3	-7.34	-16.3	-124					49.2
D1e											
D2a		296					-0.1				
D2b	5.63		78.4								0.52
D2c	4.89		35	-8.00							1.36
D2d											
D3a		294					-2.8				
D3c				-8.05							
D3d											
D4a	4.98		4.1	-9.58							4.88
D4b	4.55		8.1		-18.4	-139					5.02
D4c											
D5a	6.82		59				-0.6	-29.6	-19.4	-19.7	2.73
D5d	6.91		76	-6.95	-16.4	-119					2.13
D5e				-7.10							
D5g	6.88				-16.1	-117					
D9a		295		-7.75			-0.1				
D9b	4.29		3.19								88.4

vs. V-PDB, significantly more negative than those of C_2H_6 and C_3H_8 (-19.4% and -19.7% vs. V-PDB, respectively) measured in the same gas sample.

5. Discussion

5.1. Origin of waters

The primary source(s) of water from thermal springs and the chemical-physical processes able to cause their $^{18}\text{O}/^{16}\text{O}$ and/or $^2\text{H}/^1\text{H}$ fractionation can be investigated by comparing the $\delta^{18}\text{O-H}_2\text{O}$ and $\delta\text{D-H}_2\text{O}$ measured data with the isotope composition of meteoric water (e.g. Giggenschbach, 1991a). In the $\delta\text{D-H}_2\text{O}$ vs. $\delta^{18}\text{O-H}_2\text{O}$ diagram (Fig. 3), the Domuyo thermal waters plot on an alignment diverging from the local meteoric water line (LMWL; Hoke et al., 2013). Considering that meteoric water recharging the deep aquifer mostly permeated at an altitude

higher than the fluid discharges (from 1739 to 3144 m a.s.l.), the $\delta^{18}\text{O-H}_2\text{O}$ and $\delta\text{D-H}_2\text{O}$ values were likely deriving from (i) steam loss and (ii) water-rock isotopic exchange. The latter process is efficient at temperatures > 150 °C (Truesdell and Hulston, 1980), which are consistent with the relatively high outlet temperatures of the thermal discharges, as well as with the preliminary evaluations of reservoir temperatures (190–230 °C) based on the Na^+/K^+ geothermometer (Chiodini et al., 2014). On the other hand, the occurrence of steam loss is supported by the relatively high ^{18}O - and D-enrichments of the high temperature springs with respect to those shown by the thermal waters having lower temperatures (Fig. 3). Moreover, the $\delta^{18}\text{O}$ and δD values of water vapor (H_2O_v) in the D1d, D4b and D5d fumaroles were lighter than those of parent liquid water (Fig. 3), a feature that is consistent with isotope fractionation during steam-liquid separation. Assuming 1) the Rayleigh model for the isotopic fractionation of vapors affected by condensation and 2) the liquid-vapor isotope fractionation factors (α) for ^{18}O - ^{16}O and D-H proposed by Horita and Wesolowski (1994), the trending line describing the isotopic fractionation caused by loss of liquid water can be computed, as follows:

$$\delta = (\delta_i + 1000) F^{\alpha-1} - 1000 \tag{2}$$

where δ is the delta notation of D/H- H_2O_v and $^{18}\text{O}/^{16}\text{O}$ - H_2O_v . As shown in Fig. 3, the slightly negative ^{18}O -shift shown by the D4b and D5d samples can only be explained by admitting that condensation mostly occurred at $T < 100$ °C, i.e. at the fumarolic vent. According to these considerations, the presence of “andesitic” water (Taran et al., 1989; Giggenschbach, 1992a) was likely negligible, being masked by secondary processes. The relatively high $\delta\text{D-H}_2\text{O}$ and $\delta^{18}\text{O-H}_2\text{O}$ values of the cold waters (Fig. 3) may be due to their relatively low altitude (<1670 m a.s.l.; Table 1). The Tritium contents of the thermal waters (1.7–2.3 UT; JICA, 1984) indicated a relatively short circulation pattern of meteoric water feeding the hydrothermal aquifer, confirming that the recharge area was mainly related to the Domuyo volcanic complex. The concentrations of the main chemical constituents of the thermal waters, i.e. Na^+ and Cl^- , were stoichiometrically equivalent (Fig. 4a), as expected for typical geothermal brines (e.g. Giggenschbach, 1997a). Dilution by meteoric water affected, at various degrees, the uprising deep fluids, which mostly emerge in correspondence of creeks fed by snow melting. Noteworthy, the D9b thermal water showed the highest salinity (5884 mg/L), notwithstanding its relatively low temperature (40 °C; Table 1). The decoupling between chemistry and outlet temperature of this thermal manifestation was likely caused by its low output

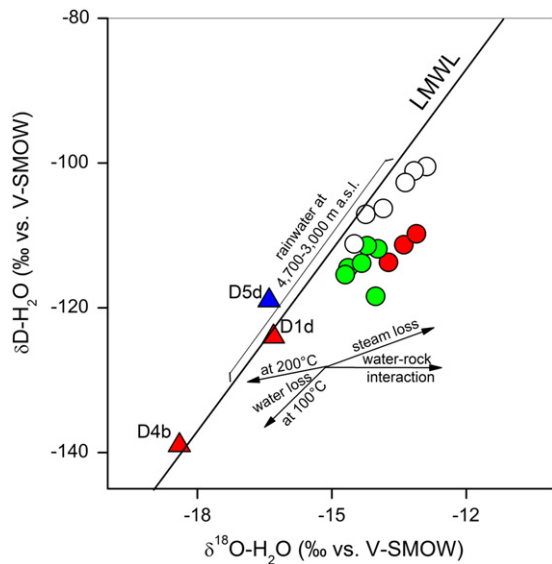


Fig. 3. $\delta\text{D-H}_2\text{O}$ vs. $\delta^{18}\text{O-H}_2\text{O}$ binary diagram for cold and thermal waters from the Domuyo volcanic complex. The Local Meteoric Water Line (LMWL; $\delta^2\text{H} = 8.15 \times \delta^{18}\text{O} + 15.3$; Hoke et al., 2013) is also shown. Symbols as in Fig. 1.

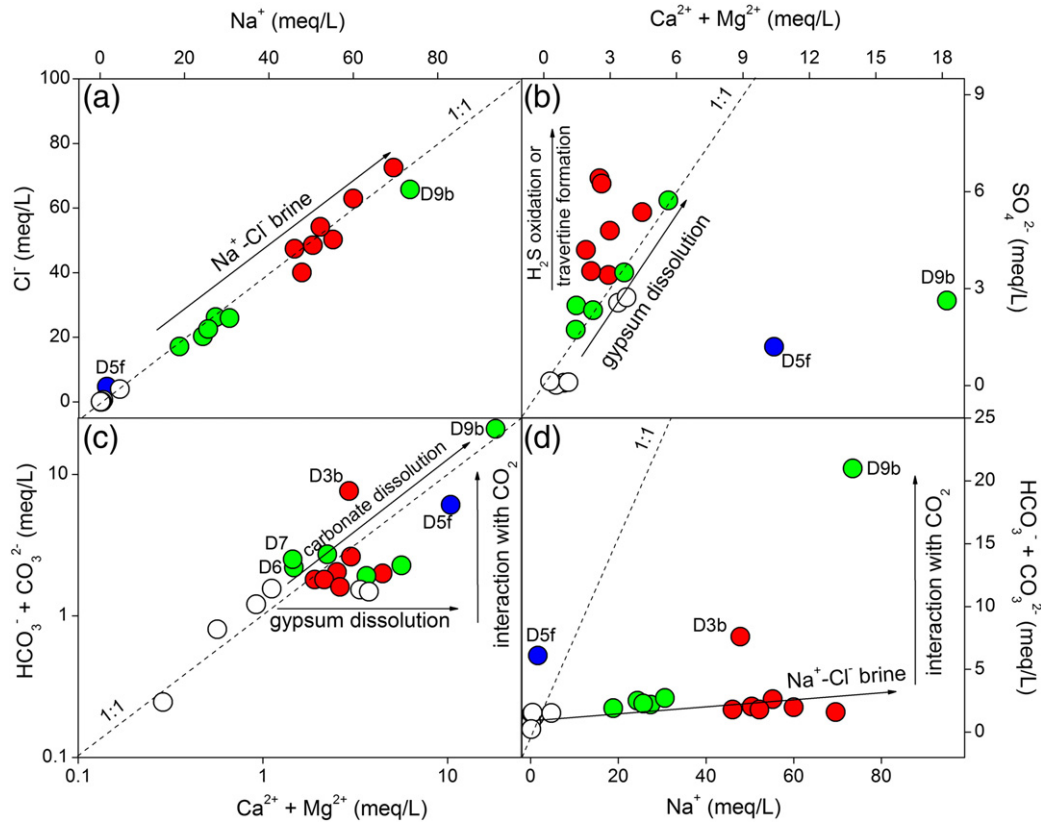


Fig. 4. (a) Cl^- vs. Na^+ , (b) SO_4^{2-} vs. $(\text{Ca}^{2+} + \text{Mg}^{2+})$, (c) $(\text{HCO}_3^- + \text{CO}_3^{2-})$ vs. $(\text{Ca}^{2+} + \text{Mg}^{2+})$, and (d) $(\text{HCO}_3^- + \text{CO}_3^{2-})$ vs. Na^+ binary diagrams for cold and thermal waters from the Domuyo volcanic complex. Concentrations are in meq/L. Symbols as in Fig. 1.

flux, favouring an efficient cooling, and its location, i.e. far from creeks (Fig. 1), thus preventing mixing with running waters that affected the other hydrothermal fluid discharges. The $(\text{SO}_4^{2-})/(\text{Ca}^{2+} + \text{Mg}^{2+})$ mol-ratios of most thermal waters were >1 (Fig. 4b). Such relatively high SO_4^{2-} concentrations, i.e. higher than those expected assuming that this ionic species completely derived from the dissolution of gypsum that was recognized upstream of the study area (Palacio and Llambias, 1978), was likely caused by the addition of SO_4^{2-} produced at shallow depth by oxidation of H_2S . Clues of the presence of this gas compounds were still recognizable in some gas discharges (Table 2). Loss of Ca^{2+} due to precipitation of travertine, whose presence was frequently observed in the emission areas, may also have contributed to increase the $\text{SO}_4^{2-}/\text{Ca}^{2+}$ ratios. As shown in Figs. 4c–d, carbonate dissolution and interaction of waters with CO_2 are the main sources for HCO_3^- and CO_3^{2-} . The latter process seems to be particularly efficient for the D3b, D6 and D7 and D9b waters that were characterized by $(\text{HCO}_3^- + \text{CO}_3^{2-})/(\text{Ca}^{2+} + \text{Mg}^{2+})$ mol-ratios >1 (Fig. 4c). The distinct chemical features of the high temperature Bramadora water (D5f), mainly consisting of low Na^+ and Cl^- concentrations (Fig. 4a) and relatively high Ca^{2+} and HCO_3^- concentrations (Fig. 4b–d), suggest that it mainly originated by steam condensation and dissolution of CO_2 -dominated gases, with negligible contribution from the geothermal brine.

As far as the minor chemical species are concerned, both Li^+ , typically depending on water-rock interaction, and B, having a strong affinity with the vapor phase, show a linear correlation with Cl^- (Fig. 5a,b). This confirms that the geochemical features of the thermal waters were related to mixing processes between a mature and hot geothermal brine and meteoric water. The relatively low B/ Cl^- ratios (Fig. 5b), i.e. significantly lower than those typically found in fluids from geothermal systems (e.g. Wairakei, New Zealand and Miravalles, Costa Rica; Giggenbach, 1991b), were likely caused by loss of B-rich steam, especially affecting those waters at the boiling temperature.

Dissolved SiO_2 , whose concentrations at $T > 150^\circ\text{C}$ depends on the solubility of quartz, can be used to estimate equilibrium temperatures according to two different equations (Fournier and Potter, 1982), as follows:

$$T(\text{K}) = 1390 / (5.19 - \log \text{SiO}_2) \quad (3)$$

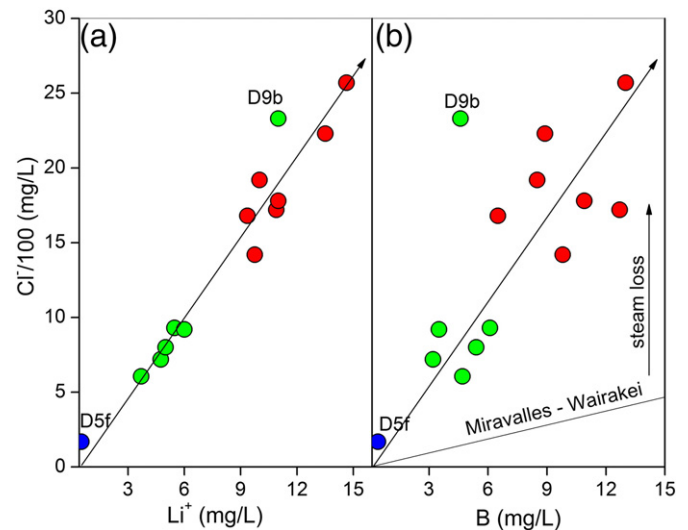


Fig. 5. (a) Cl^- vs. Li^+ and (b) Cl^- vs. B binary diagrams for cold and thermal waters from the Domuyo volcanic complex. Concentrations are in mg/L. The Cl^-/B ratios of hydrothermal waters from Miravalles volcano (Costa Rica and Wairakei (New Zealand)) (Giggenbach, 1991b) are also reported. Symbols as in Fig. 1.

and

$$T(K) = 1522 / (5.75 - \log \text{SiO}_2) \quad (4)$$

Using Eq. (4), which is the most appropriate for the $\text{Na}^+ - \text{Cl}^-$ boiling waters that were likely affected by loss of steam, and Eq. (3) for the other thermal waters, the calculated T_{SiO_2} values ranged from 148 to 181 °C (Table 1). These values are significantly lower than those preliminary estimated by Chiodini et al. (2014) on the basis of the cation exchange reaction between albite and K-feldspar (Giggenbach, 1988), which were confirmed by using the data of this study (from 182 to 249 °C; Fig. 6 and Table 1). Hence, the silica calculated temperatures significantly decreased due to both dilution and cooling affecting the thermal discharges approaching the surface. As suggested by Giggenbach (1988), PCO_2 in geothermal fluids is likely controlled by the conversion of Ca-Al silicates to calcite, involving the formation of K-mica. The K^2/Ca ratios related to this process, which is independent on temperature, represent a suitable PCO_2 -indicator. Thus, combining the K^2/Ca and the K^2/Mg ratios, the latter being used in Fig. 6 as the fast responding geothermometer (Giggenbach, 1988), we obtain a binary diagram describing the relationship between PCO_2 and the equilibrium temperatures indicated by the K-Mg geothermometer. According to this approach (Fig. 7), the hypothesized mineral-solution interaction seems to efficiently control PCO_2 of the Domuyo thermal waters. The slight shift to higher K^2/Ca ratios with respect to the PCO_2 equilibrium curve was likely caused by Ca^{2+} loss produced by travertine deposition, a process already invoked to explain the SO_4^{2-} -excess (Fig. 4b).

5.2. Origin of gases

The relatively high N_2 , Ar and O_2 concentrations characterizing most CO_2 -dominated gas emissions of the study area (D1, D2, D3, D4, D9, D18, D19 and D20) emerging at the foothill of the Cerro Domuyo (Fig. 1) suggest a strong air contribution. The N_2/O_2 ratios (from 3.7 to 14.3), slightly higher than that of air (Fig. 8a), indicate addition of air at relatively shallow depth since hydrothermal fluids are typically O_2 -free. Such an air addition was likely caused by the interaction of the uprising

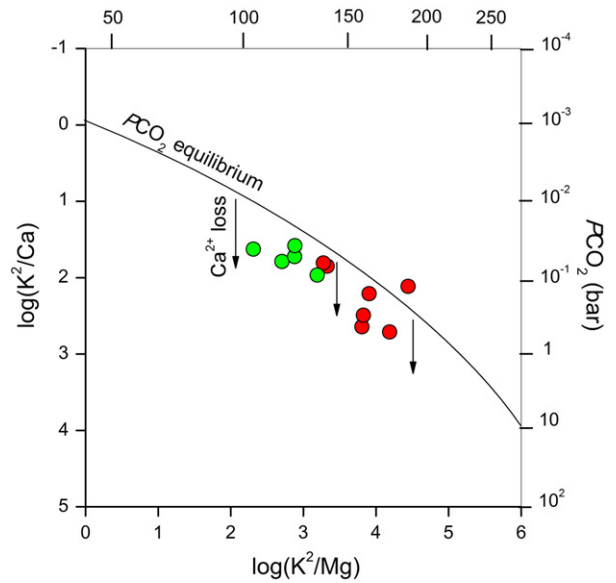


Fig. 7. $\log(\text{K}^2/\text{Ca})$ vs. $\log(\text{K}^2/\text{Mg})$ binary diagram for gases from the Domuyo volcanic complex. The PCO_2 equilibrium curve, calculated according to Giggenbach (1988) is reported. Symbols as in Fig. 1.

hydrothermal fluids with an air-saturated meteoric aquifer, although some air contamination occurring during the gas sampling cannot be excluded. The low N_2/Ar ratios (<50), i.e. between those of ASW (from 39 to 41 at 40–90 °C) and air (82), and the $^{40}\text{Ar}/^{36}\text{Ar}$ ratios (~295; i.e. consistent with that of air) seem to exclude a significant N_2 and Ar extra-atmospheric contribution, a hypothesis that conflicts with the negative $\delta^{15}\text{N}$ values (from -0.1 to -3.1‰ vs. air). Considering that a variety of gases from arc volcanoes, as well as those of N_2 produced by reactions involving metasedimentary rocks, are characterized by positive $\delta^{15}\text{N}$ values (Haendel et al., 1986; Sano et al., 2001; Fischer et al., 2002; Li et al., 2007; Busigny et al., 2011), the occurrence of a significant extra-atmospheric N_2 contribution from the crust and/or recycled subducted sediments seems unlikely. On the contrary, the measured $\delta^{15}\text{N}$ values were consistent with those of (i) fluids released from the upper mantle (-6‰ vs. air; Javoy et al., 1986; Marty and Zimmermann, 1999; Sano et al., 2001; Inguaggiato et al., 2004), and (ii) crustal N_2 produced by degradation of immature organic matter (Zhu et al., 2000). The occurrence of negative $\delta^{15}\text{N}$ values in gases showing air(ASW)-like N_2/Ar ratios was already observed in gas discharged

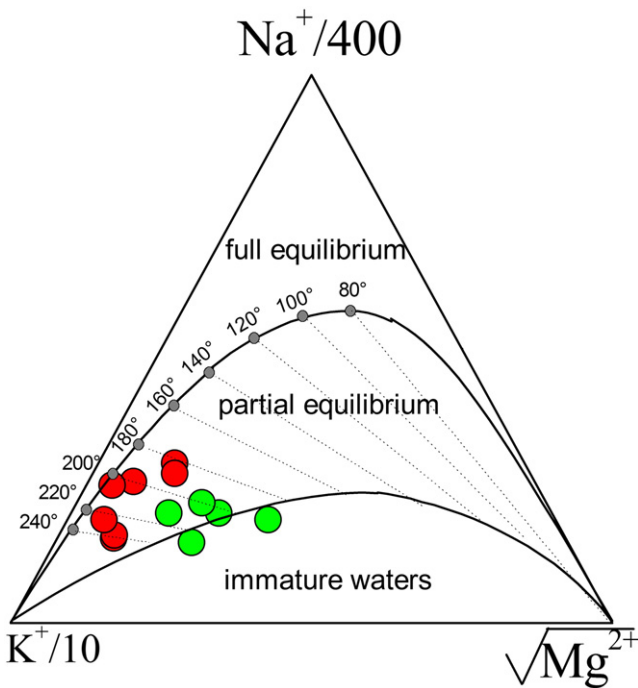


Fig. 6. $\text{Mg}^{2+} - \text{Na}^+ - \text{K}^+$ ternary diagram for gases from the Domuyo volcanic complex. The full and partial equilibrium curves, calculated according to Giggenbach (1988), are reported. Symbols as in Fig. 1.

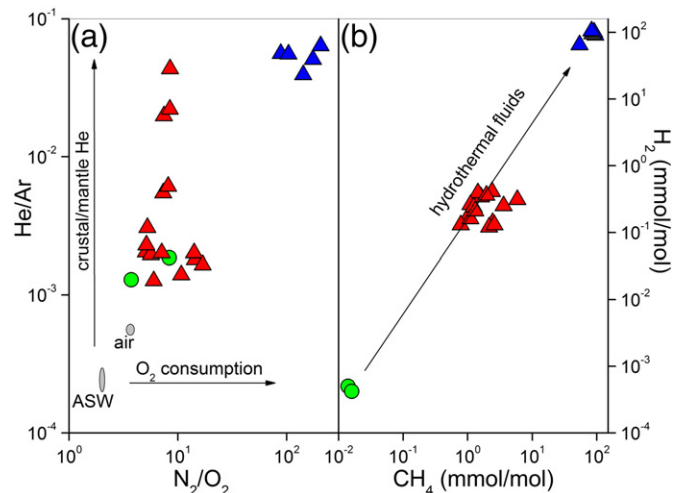


Fig. 8. (a) He/Ar vs. N_2/O_2 and (b) H_2 vs. CH_4 binary diagrams for gases from the Domuyo volcanic complex. Concentrations are in mmol/mol. Symbols as in Fig. 1.

from Rungwe Volcanic Province (Tanzania), and interpreted as related to the contribution of sub-continental lithospheric mantle volatiles (de Moor et al., 2013). Similarly, hydrothermal fluids from Yellowstone (USA) showed isotopic evidences of extra-atmospheric N₂ notwithstanding their low N₂/Ar ratios, suggesting the occurrence of a deep end-member whose N₂/Ar ratio resembled that of air (Chiodini et al., 2012). However, it is worth to mention that both Rungwe Volcanic Province and Yellowstone gas discharges are belonging to an extensional regime and a plume generated continental hot-spot, respectively, whereas those at Domuyo are from a typical subduction-related area. This suggests that further work is needed to satisfactory explain the apparent contradiction between gas composition and N₂ isotopes. Consequently, we may speculate that the lack of significant N₂-excess and the negative δ¹⁵N values of the Domuyo gases were related to a mantle source characterized by low N₂/Ar ratio. Air contamination from meteoric contribution, indicated by the relatively low N₂/O₂ ratios (Fig. 8a), was evidently not able to completely mask the deep isotopic N₂ signature.

The high He/Ar ratios, which were up to two orders of magnitude higher than that of air (Fig. 8a), coupled with the widely varying R/Ra values (from 1.86 to 4.98; Table 3), pointed to extra-atmospheric He likely deriving from both crustal and mantle sources locally prevailing each other. The δ¹³C-CO₂ values are within the lower range typical for mantle-derived fluids (~−4 to −8‰ vs. V-PDB; Pineau and Javoy, 1983; Javoy et al., 1986; Taylor, 1986; Hoefs, 1997). However, the relatively high CO₂/³He ratios (Table 3), which in some cases are one order of magnitude higher than that of MORB gases (1.2 × 10⁹; Marty and Jambon, 1987), indicate the occurrence of crustal CO₂. The latter possibly derived from organic matter degradation occurring at shallow depth and/or related to the subduction of C-bearing material. On the other hand, relatively low CO₂/³He ratios, such as that measured in D2b (0.52 × 10⁹; Table 3) may point to the occurrence of CO₂-loss due to dissolution in the shallow waters. In fact, at high pH values (>7) this process is able to cause a significant ¹³C-¹²C fractionation in CO₂ (Gilfillan et al., 2009), such as those measured in the Domuyo thermal waters (Table 1). Notably, the δ¹³C-TDIC values from the D1b, D2b and D3b thermal waters (from −11.9 to −13‰ vs. V-PDB) were significantly lower than those of CO₂ in the corresponding high temperature gases (Table 2). This implies that the attainment of the CO₂-TDIC isotopic equilibrium occurred at temperatures >250 °C (Deines et al., 1974), i.e. likely too high for this hydrothermal system (Chiodini et al., 2014). Mixing of deep fluids with shallow waters, the latter being typically showing ¹²C-rich dissolved carbonate species, may explain such a low isotopic signature characterizing TDIC.

The Bramadora gases (D5a–e) were characterized by a peculiar chemical and isotopic composition. The occurrence of H₂S and CO, which were absent or at very low concentrations in the other gas discharges (Table 2), relatively high H₂ and CH₄ concentrations (Fig. 8b), as well as low abundances of atmospheric gases (Fig. 8a), were consistent with the typical compositional features of hydrothermal fluids (e.g. Giggenbach, 1991b). The R/Ra values of D5a and D5d were the highest measured at Domuyo (Table 3) and similar to those measured in fumaroles from active volcanoes of the SVZ (e.g. Hilton et al., 1993; Agosto et al., 2013; Benavente et al., 2013; Tassi et al., 2016). Assuming a three-component mixing model between atmosphere, mantle and crust components having R/Ra equal to 1, 8 and 0.02, respectively (Hilton et al., 2002), they indicate a contribution of mantle-derived He up to 86%. Such a high mantle He fraction is a clear evidence of a significant magmatic gas contribution to the hydrothermal system. This evidence appears quite unexpected for a volcanic system that is considered extinct. The lack of other clues of magma degassing in the discharged fluids, e.g. the presence of highly acidic gases (SO₂, HCl, HF), was likely due to efficient scrubbing processes (Symonds et al., 2001), representing an indirect proof for the occurrence of a well-developed hydrothermal fluid source. A further important peculiar chemical feature of the D5a–e gases is represented by their relatively high N₂/

Ar ratios (up to 130), as commonly found in gas discharges associated with subduction-zone andesitic magmatism (Giggenbach, 1992b), being related to N₂ extraction from subducted slab and sediments (Snyder et al., 2003). As already mentioned, the negative δ¹⁵N₂ values of the Domuyo gases suggest that the N₂-excess in this system was produced by an organic source. However, considering the strong He mantle signature of the D5a gas sample, it cannot be excluded that the isotope signature of the local magmatic N₂ source (−0.6‰ vs air; Table 3) is close to the atmospheric value.

The carbon isotopic signature of CH₄ in D5a (−26.9‰ vs. V-PDB), combined with the less negative δ¹³C values of C₂H₆ and C₃H₈, points to a thermogenic origin of the hydrocarbons (e.g. Chung et al., 1988; Galimov, 1988, 2006). The relatively high CH₄/(C₂H₆ + C₃H₈) ratios (up to 930) are quite unusual for thermogenic hydrocarbons (e.g. Whiticar, 1999). Based on the laboratory experiments performed by Berner et al. (1995), it has been postulated that primary cracking of organic matter under open system conditions can yield high CH₄/(C₂H₆ + C₃H₈) ratios with respect to those typical of thermogenic gases, as well as convergent carbon isotope patterns between the C₂₊ hydrocarbons (Lorant et al., 1998; Fiebig et al., 2015). Hence, a lack of carbon isotope fractionation between C₂H₆ and C₃H₈, as observed for sample D5a, may support a thermogenic origin for these organic gas species.

5.3. Gas geothermometry

Geothermometric calculations based the redox independent geothermometer proposed by Chiodini and Marini (1998) can be carried out using the Bramadora gases (D5a–e) only, since CO concentrations in the other Domuyo gas discharges were below the detection limit (Table 2). Gas equilibria in the H₂-H₂O-CO₂-CO-CH₄ system are controlled by the following independent reactions:



As depicted in the [$\log(X_{\text{CO}}/X_{\text{CO}_2}) + \log(X_{\text{H}_2\text{O}}/X_{\text{H}_2})$] vs. [$3\log(X_{\text{CO}}/X_{\text{CO}_2}) + \log(X_{\text{CO}}/X_{\text{CH}_4})$] binary diagram (Fig. 9), the D5a–e gases plot

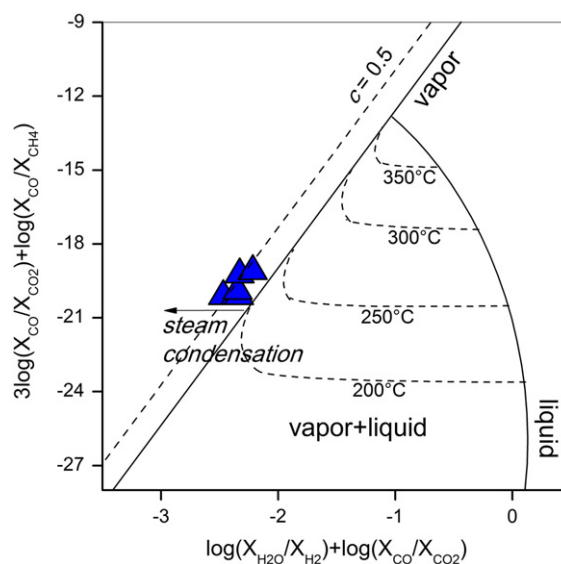


Fig. 9. [$\log(X_{\text{CO}}/X_{\text{CO}_2}) + \log(X_{\text{H}_2\text{O}}/X_{\text{H}_2})$] vs. [$3\log(X_{\text{CO}}/X_{\text{CO}_2}) + \log(X_{\text{CO}}/X_{\text{CH}_4})$] binary diagram for the D5a–e gases from the Domuyo volcanic complex. The theoretical compositions of (1) single saturated vapor phase (vapor), (2) single saturated liquid phase (liquid), and (3) single saturated vapor phase after separation at $T = 100$ °C of different fractions (c) of condensed steam (dashed line), are reported. Symbols as in Fig. 1.

to the left of the theoretical composition of a single saturated vapor phase (vapor) equilibrated at 200–225 °C. The departure from the single saturated vapor phase line could be due to condensation (c) of a significant fraction (up to 0.5) of steam, a process consistent with the outlet temperatures of the fumaroles (Table 2) and also indicated by the $\delta^{18}\text{O}\text{-H}_2\text{O}$ and $\delta\text{D}\text{-H}_2\text{O}$ values (Fig. 3). Assuming that redox conditions are correctly described by the FeO-FeO_{1.5} buffer, which is regarded as the typical redox (rock) buffer for hydrothermal fluids (Giggenbach, 1987) and are consistent with the measured $\log(X_{\text{H}_2}/X_{\text{H}_2\text{O}})$ ratios (from -2.71 to -2.92), gas geothermometry in the H₂-H₂O-CO₂-CO system can also be investigated. The D5a-e gases in the $\log(X_{\text{H}_2}/X_{\text{H}_2\text{O}})$ vs. $\log(X_{\text{CO}}/X_{\text{CO}_2})$ diagram (Fig. 10) plot close to the line of equilibrated vapor at 170–190 °C, i.e. at temperatures lower than those indicated in Fig. 9. On the contrary, geothermometric calculations in the CO₂-CH₄-C₃H₆-C₃H₈ system (e.g. Fiebig et al., 2013), at redox conditions similar than those adopted for the H₂-CO pair, suggest that the Bramadora gases equilibrated in a liquid phase at 210–220 °C (Fig. 11). This difference is likely related to (i) cooling of the vapors produced from the boiling of the hydrothermal aquifer and (ii) the slower kinetics of the C₃H₆-C₃H₈ and CH₄-CO₂ reactions with respect to those characterizing the reactions between the CO-CO₂ and H₂/H₂O pairs (Giggenbach, 1997b; Fiebig et al., 2013). It is worth noting that the other Domuyo gas discharges plot far from equilibrium conditions (Fig. 11), confirming that processes affecting these gases at shallow depth (e.g. mixing with a meteoric aquifer) significantly changed their chemical features.

The calculated temperature from carbon isotope equilibrium between CO₂ and CH₄ (~340 °C; Horita, 2001), computed using the only available $\delta^{13}\text{C}\text{-CH}_4$ value (D5a) coupled with the $\delta^{13}\text{C}\text{-CO}_2$ values of D5d and D5e gases (Table 3), is in strong disagreement with those indicated by the water and gas chemical composition and seems too high for this hydrothermal system. The lack of complete equilibrium between the carbon stable isotopes of CH₄ and CO₂, a process that is typically characterized by a very slow kinetics (Giggenbach, 1997b), may explain such unrealistic estimated temperature.

5.4. Geochemical conceptual model

The complete geochemical dataset reported in this study provided detailed insights into the origin of the various chemical constituents of

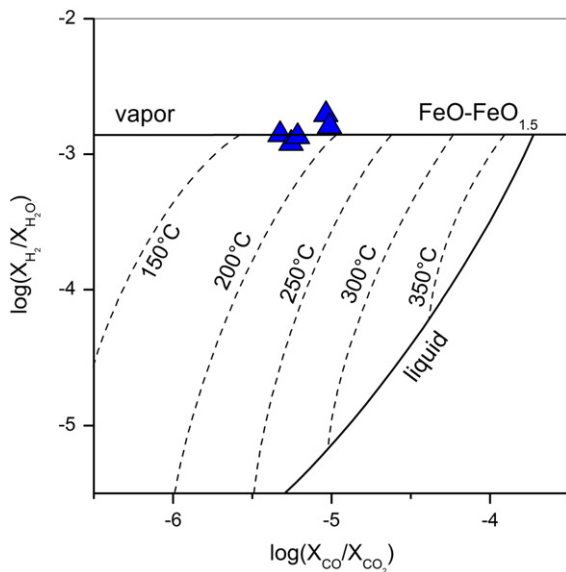


Fig. 10. $[\log(X_{\text{H}_2}/X_{\text{H}_2\text{O}})]$ vs. $[\log(X_{\text{CO}}/X_{\text{CO}_2})]$ binary diagram for the D5a-e gases from the Domuyo volcanic complex. The theoretical compositions of (1) single saturated vapor phase (vapor), (2) single saturated liquid phase (liquid), at under the control of the FeO-FeO_{1.5} redox buffer (Giggenbach, 1987), are also reported. Symbols as in Fig. 1.

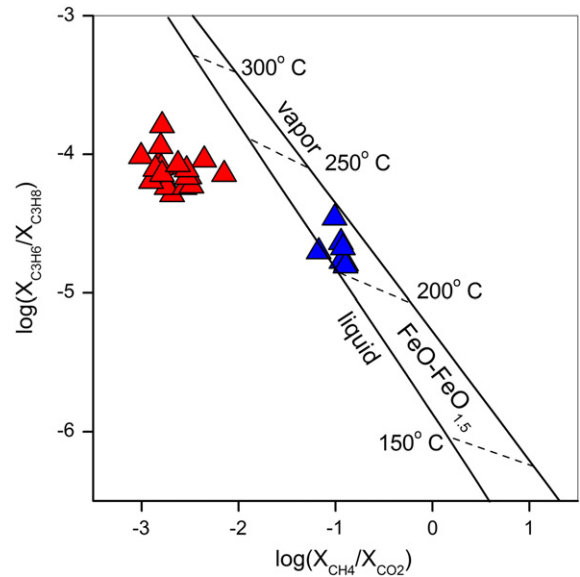


Fig. 11. $[\log(X_{\text{C}_3\text{H}_6}/X_{\text{C}_3\text{H}_8})]$ vs. $[\log(X_{\text{CH}_4}/X_{\text{CO}_2})]$ binary diagram for gases from the Domuyo volcanic complex. The theoretical compositions of (1) single saturated vapor phase (vapor), (2) single saturated liquid phase (liquid), at under the control of the FeO-FeO_{1.5} redox buffer (Giggenbach, 1987), are also reported. Symbols as in Fig. 1.

the thermal fluid discharges and the chemical-physical conditions of the hydrothermal source, as depicted by the conceptual geochemical model reported in Fig. 12. Gas geothermometry based on the composition of the slow-reacting C₃ hydrocarbons in a liquid phase pointed to ~220 °C, i.e. in the range (up to 240 °C) of the temperatures indicated by the Na⁺-K⁺ ratios. These thermal conditions likely characterize the hydrothermal reservoir at 400–600 m depth, whose occurrence was indicated by past geophysical surveys (JICA, 1983, 1984). At the estimated temperature, the gas (mainly CO₂) pressure is in the order of few tens of bars (Keenan et al., 1969), thus too low to allow the direct uprising of fluids from 2 to 3 km depth where a second aquifer is possibly hosted within the volcanic rock basement. According to fast responding geothermometers (H₂-H₂O and CO-CO₂), gases produced by boiling of the shallower reservoir re-equilibrate at 170–190 °C. Heat and CO₂- and ³He-rich fluids are likely provided by a still actively degassing magma batch located at an unknown depth, whereas the water recharge is mostly deriving from local rain and melting of the glaciers permanently occupying the summit of the volcanic complex. Magmatic gases (e.g. SO₂, HCl, HF) from the magmatic source dissolve within the hydrothermal aquifer(s) to produce SO₄²⁻, Cl⁻ and F⁻. Reducing conditions caused by the interaction between the hydrothermal/magmatic fluids and the hosting rocks favor the production of H₂S, CO and CH₄. The primary origin of CH₄, as well as the higher hydrocarbons, is also possibly related to thermal degradation of mature organic matter leached from sediments by the recharging meteoric water. Most gas discharges located at the base of Cerro Domuyo are affected by dilution and air contamination due to mixing with meteoric water of the creeks whose pattern is driven by the structural setting controlling the hydrothermal fluid uprising. Fluids discharged from the Bramadora emissions are less affected by contamination of running waters, likely due to their high altitude. Thus, their geochemical features approach those of the deep fluids: (i) low concentrations of air compounds, (ii) relatively high concentrations of the typical hydrothermal gases and (iii) magmatic He and CO₂ isotopic signatures.

6. Conclusions

The chemical features of the Domuyo thermal fluid discharges are consistent with the occurrence of a well-developed hydrothermal

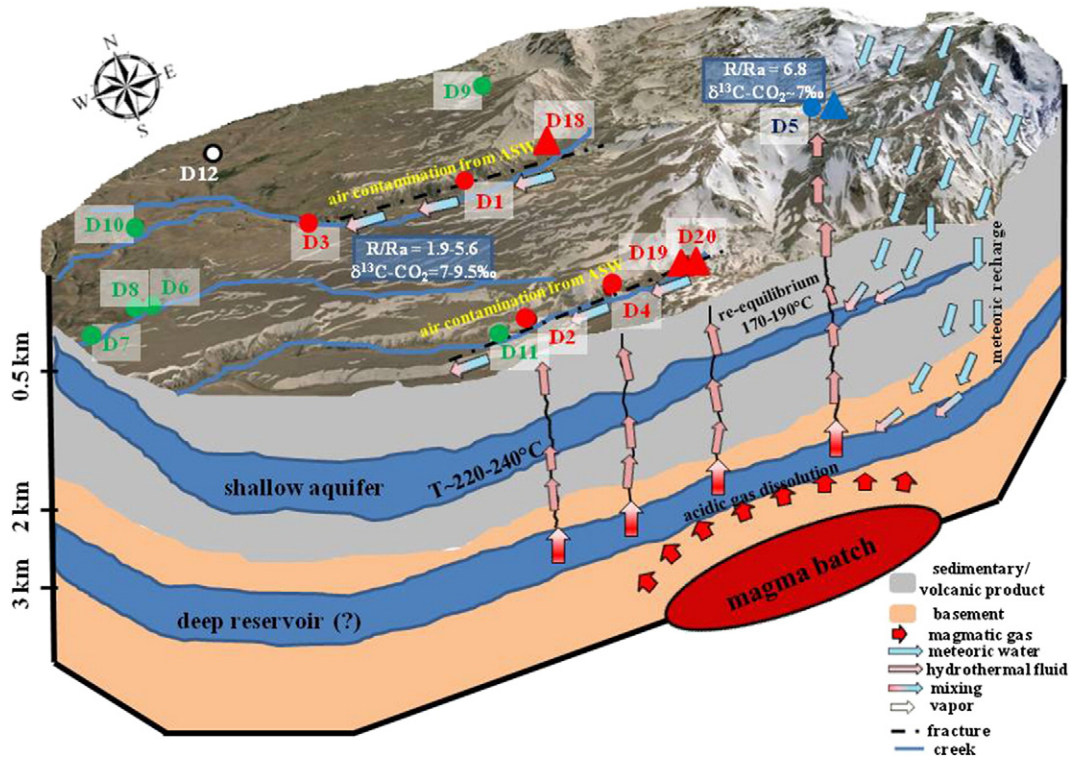


Fig. 12. Three-dimensional geochemical conceptual model of the hydrothermal system of the Domuyo volcanic complex.

system, where (i) permeating meteoric water, (ii) fluids from a deep heat source and (iii) rocks interact to produce Cl-rich waters and reduced gas compounds. The hydrothermal fluids emerging at the foothill of Cerro Domuyo (1900–2200 m a.s.l.) mix with running waters, a process that controls their outlet temperatures and causes water dilution and contamination of air compounds. Notwithstanding, clear clues of magmatic degassing, basically consisting of high R/Ra values, were recognized in the fluid discharges located at higher altitude (~3150 m a.s.l.), where mixing with the meteoric aquifer is not significant. Gas and solute geothermometers consistently suggest the occurrence of a relatively shallow hydrothermal reservoir characterized by medium-enthalpy conditions, likely masking the chemical-physical conditions of the deeper aquifer hypothesized by JICA (1983, 1984). The occurrence of an alternative energy source at the Domuyo volcanic complex represents an interesting opportunity for the economical development of this remote region of the Andes. However, a reliable estimation of the total geothermal potential, the assessment of depth and dimensions of the main fluid reservoir, possibly carrying out detailed geophysical measurements, still remain a challenge, although the huge amount of thermal energy released from the thermal discharges indirectly testifies to the importance of this resource.

Acknowledgements

We would like to thank M. de Moor whose constructive comments significantly improved this manuscript. The Authors wish also to express their gratitude to the personnel of the Domuyo Provincial Park for their fundamental help to the fieldwork activity. This work was supported by the laboratories of Fluid Geochemistry and Stable Isotopes of the Department of Earth Sciences of the University of Florence and CNR-IGG. Participation of Jens Fiebig has been enabled through DFG fund FI-948/6-1. The authors also thank Dr. Andrea Rizzo for the analysis of He isotopes carried out at the INGV laboratories of Palermo (Italy) and Enrico Calvi for the measurements of the carbon ratios in CO₂.

References

- Agusto, M., Tassi, F., Caselli, A.T., Vaselli, O., Rouwet, D., Capaccioni, B., Caliro, S., Chiodini, G., Darrah, T., 2013. Gas geochemistry of the magmatic-hydrothermal fluid reservoir in the Copahue-Caviahue Volcanic Complex (Argentina). *J. Volcanol. Geotherm. Res.* 257, 44–56.
- Benavente, O., Tassi, F., Gutiérrez, F., Vaselli, O., Aguilera, F., Reich, M., 2013. Origin of fumarolic fluids from Tupungatito Volcano (Central Chile): interplay between magmatic, hydrothermal, and shallow meteoric sources. *Bull. Volcanol.* 75 (8), 1–15.
- Bencini, A., 1985. Applicabilità del metodo dell'Azometina-H alla determinazione del boro nelle acque naturali. *Rend. Soc. It. Miner. Petrol.* 40, 311–316.
- Berner, U., Faber, E., Scheeder, G., Panten, D., 1995. Primary cracking of algal and landplant kerogen: kinetic models of isotope variations in methane, ethane, and propane. In: Rice, D.D., Schoell, M. (Eds.), *In: Processes of Natural Gas Formation*. Chem. Geol. 126, pp. 233–245.
- Busigny, V., Cartigny, P., Philippot, P., 2011. Nitrogen isotopes in ophiolitic metagabbros: a re-evaluation of modern nitrogen fluxes in subduction zones and implication for the early Earth atmosphere. *Geochim. Cosmochim. Acta* 75, 7502–7521.
- Chiodini, G., Marini, L., 1998. Hydrothermal gas equilibria: the H₂O-H₂-CO₂-CO-CH₄ system. *Geochim. Cosmochim. Acta* 62, 2673–2687.
- Chiodini, G., Caliro, S., Lowenstern, J.B., Evans, W.C., Bergfeld, D., Tassi, F., Tedesco, D., 2012. Insights from fumarole gas geochemistry on the origin of hydrothermal fluids on the Yellowstone Plateau. *Geochim. Cosmochim. Acta* 89, 265–278.
- Chiodini, G., Liccioli, C., Vaselli, O., Calabrese, S., Tassi, F., Caliro, S., Caselli, A.T., Agusto, M., D'Alessandro, W., 2014. The Domuyo volcanic system: an enormous geothermal resource in Argentine Patagonia. *J. Volcanol. Geotherm. Res.* 274, 71–77.
- Chung, H.M., Gormly, J.R., Squires, R.M., 1988. Origin of gaseous hydrocarbons in subsurface environments: theoretical considerations of carbon isotope distribution. *Chem. Geol.* 71, 97–103.
- Coleman, M.L., Shepherd, T.J., Durham, J.J., Rouse, J.E., Moore, G.R., 1982. Reduction of water with zinc for hydrogen isotope analysis. *Anal. Chem.* 54, 993–995.
- de Moor, J.M., Fischer, T.P., Sharo, Z.D., Hilton, D.R., Barry, P.H., Mangasini, F., Ramirez, C., 2013. Gas chemistry and nitrogen isotope compositions of cold mantle gases from Rungwe Volcanic Province, southern Tanzania. *Chem. Geol.* 339, 30–42.
- Deines, P., Langmuir, D., Harmon, R.S., 1974. Stable carbon isotope ratios and the existence of a gas phase in the evolution of carbonate ground waters. *Geochim. Cosmochim. Acta* 38, 1147–1164.
- Epstein, S., Mayeda, T.K., 1953. Variations of the ¹⁸O/¹⁶O ratio in natural waters. *Geochim. Cosmochim. Acta* 4, 213.
- Evans, W., White, L., Rapp, J., 1998. Geochemistry of some gases in hydrothermal fluids from the southern Juan de Fuca Ridge. *J. Geophys. Res.* 103, 305–313.
- Fariás, M., Comte, D., Charrier, R., Martinod, J., David, C., Tassara, A., Tapia, F., Fock, A., 2010. Crustal-scale structural architecture in central Chile based on seismicity and surface geology: implications for Andean mountain building. *Tectonics* 29, 22.

- Fiebig, J., Tassi, F., D'Alessandro, W., Vaselli, O., Woodland, A.B., 2013. Carbon-bearing gas geothermometers for volcanic–hydrothermal systems. *Chem. Geol.* 351, 66–75.
- Fiebig, J., Tassi, F., D'Alessandro, W., Vaselli, O., Woodland, A.B., 2015. Isotopic patterns of hydrothermal hydrocarbons emitted from Mediterranean volcanoes. *Chem. Geol.* 396, 152–163.
- Fischer, T.P., Hilton, D.R., Zimmer, M.M., Shaw, A.M., Sharp, Z.D., Walker, J.A., 2002. Subduction and recycling of nitrogen along the Central American margin. *Science* 297, 1154–1157.
- Folguera, A., Ramos, V., Zapata, T., Spagnuolo, M.G., 2007. Andean evolution at the Guañacos and Chos Malal fold and thrust belts (36°30'–37°S). *J. Geodyn.* 44, 129–148.
- Fournier, R.O., Potter, R.W., 1982. A revised and expanded silica (quartz) geothermometer. *Geoth. Res. Council Bull.* 11–10, 3–12.
- Galimov, A.M., 1988. Sources and mechanisms of formation of gaseous hydrocarbons in sedimentary rocks. *Chem. Geol.* 71, 77–95.
- Galimov, E.M., 2006. Isotope organic geochemistry. *Org. Geochem.* 37, 1200–1262.
- Giggenbach, W.F., 1987. Redox processes governing the chemistry of fumarolic gas discharges from White Island, New Zealand. *Appl. Geochem.* 2, 143–161.
- Giggenbach, W.F., 1988. Geothermal solute equilibria. *Geochim. Cosmochim. Acta* 52, 2749–2765.
- Giggenbach, W.F., 1991a. Isotopic composition of geothermal water and steam discharges. In: D'Amore, F. (Ed.), *Application of Geochemistry in Geothermal Reservoir Development*. UNITAR, New York, pp. 253–273.
- Giggenbach, W.F., 1991b. Chemical techniques in geothermal exploration. In: D'Amore, F. (Ed.), *Application of Geochemistry in Geothermal Reservoir Development*. UNITAR, New York, pp. 119–144.
- Giggenbach, W.F., 1992a. Isotopic shifts in waters from geothermal and volcanic systems along margins, and their origin. *Earth Planet. Sci. Lett.* 113, 495–510.
- Giggenbach, W.F., 1992b. The composition of gases in geothermal and volcanic systems as a function of tectonic setting. In: Kharaka, Y.K., Maest, A.S. (Eds.), *Water–Rock Interaction*. Balkema, Rotterdam, pp. 873–878.
- Giggenbach, W.F., 1997a. The origin and evolution of fluids in magmatic–hydrothermal systems. In: Barnes, H.L. (Ed.), *Geochemistry of Hydrothermal Ore Deposits*. John Wiley and Sons, New York, pp. 737–789.
- Giggenbach, W.F., 1997b. Relative importance of thermodynamic and kinetic processes in governing the chemical and isotopic composition of carbon gases in high-heatflow sedimentary basins. *Geochim. Cosmochim. Acta* 61, 3763–3785.
- Gilfillan, S.M.V., Sherwood Lollar, B., Holland, G., Blagburn, D., Stevens, S., Schoell, M., Cassidy, M., Ding, Z., Lacrampe-Couloume, G., Ballentine, C.J., 2009. Solubility trapping in formation water as dominant CO₂ sink in natural gas fields. *Nat. Lett.* 458, 614–618.
- Groeber, P., 1947. Observaciones geológicas a lo largo del meridiano 70.3, hojas Domuyo, Mari Mahuida, Huarhuar Co y parte de Epu Lauken. *Rev. Asoc. Geol. Argent.* 2 (4), 347–408.
- Haendel, D., Mohle, K., Nitzsche, H.M., Stihl, G., Wand, U., 1986. Isotopic variations of the fixed nitrogen in metamorphic rocks. *Geochim. Cosmochim. Acta* 50, 749–758.
- Hilton, D.R., Hammerschmidt, K., Teufel, S., Friedrichsen, H., 1993. Helium isotope characteristics of Andean geothermal fluids and lavas. *Earth Planet. Sci. Lett.* 120 (3–4), 265–282.
- Hilton, D.R., Fischer, T.P., Marty, B., 2002. Noble gases and volatile recycling at subduction zones. In: Porcelli, D., Ballentine, C.J., Wieler, R. (Eds.), *Noble Gases in Cosmochemistry and Geochemistry*. Mineral. Soc. Am. Washington, pp. 319–370.
- Hoefs, J., 1997. *Stable Isotope Geochemistry*. fourth ed. Springer-Verlag, Berlin, Germany, p. 201.
- Hoke, G.D., Aranibar, J.N., Viale, M., Araneo, D.C., Llano, C., 2013. Seasonal moisture sources and the isotopic composition of precipitation, rivers, and carbonates across the Andes at 32.5–35.5°S. *Geochem. Geophys. Geosyst.* 14 (4), 962–978.
- Horita, J., 2001. Carbon isotope exchange in the system CO₂–CH₄ at elevated temperatures. *Geochim. Cosmochim. Acta* 65, 1907–1919.
- Horita, J., Wesolowski, D.J., 1994. Liquid–vapor fractionation of oxygen and hydrogen isotopes of water from the freezing to the critical temperature. *Geochim. Cosmochim. Acta* 58, 3425–3437.
- Inguaggiato, S., Taran, Y., Grassa, F., Capasso, G., Favara, R., Varley, N., Faber, E., 2004. Nitrogen isotopes in thermal fluids of a forearc region (Jalisco Block, Mexico): evidence for heavy nitrogen from continental crust. *Geochem. Geophys. Geosyst.* 5, Q12003. <http://dx.doi.org/10.1029/2004GC000767>.
- Javoy, M., Pineau, F., Delorme, H., 1986. Carbon and nitrogen isotopes in the mantle. *Chem. Geol.* 57, 41–62.
- JICA, 1983. Argentine Republic. Final Report on the Northern Neuquen Geothermal Development Project. First-Second Phase Survey, No 25 .
- JICA, 1984. Argentine Republic. Final Report on the Northern Neuquen Geothermal Development Project. Third Phase Survey, No 25 .
- Kay, S.M., Abbruzzi, J.M., 1996. Magmatic evidence for Neogene lithospheric evolution of the central Andean 'flat-slab' between 30° and 32°S. *Tectonophysics* 259, 15–28.
- Kay, S.M., Ramos, V.A., Mpodozis, C., Sruga, P., 1989. Late Paleozoic to Jurassic silicic magmatism at the Gondwanaland margin: analogy to the Middle Proterozoic in North America? *Geology* 17, 324–328.
- Kay, S.M., Burns, W.M., Copeland, P., Mancilla, O., 2006. Upper Cretaceous to Holocene magmatism and evidence for transient shallowing of the Andean subduction zone under the northern Neuquen basin. In: Kay, S.M., Ramos, V.A. (Eds.), *Evolution of an Andean Margin: a Tectonic and Magmatic Perspective from the Andes to the Neuquen Basin (35°–39°S Lat.)*. *Geol. Soc. Am.* 407, pp. 19–60 Special Papers.
- Keenan, J.H., Keyes, F.G., Hill, P.G., Moore, J.G., 1969. *Steam Tables. Thermodynamic Properties of Water Including Vapor, Liquid, and Solid Phases (International System of Units-S.I.)*. Wiley, p. 162.
- Kietzmann, D.A., Vennari, V.V., 2013. Sedimentología y estratigrafía de la Formación Vaca Muerta (Tithoniano–Berriasiano) en el área del cerro Domuyo, norte de Neuquén, Argentina. *Andean Geol.* 40 (1), 41–65.
- Li, L., Bebout, G.E., Idleman, B.D., 2007. Nitrogen concentration and δ¹⁵N of altered oceanic crust obtained on ODP Legs 129 and 185: insights into alteration-related nitrore enrichment and the nitrogen subduction budget. *Geochim. Cosmochim. Acta* 71, 2344–2360.
- Llambías, E.J., Leanza, H., 2005. Depósitos laháricos en la Formación Los Molles en Chacay Melehue, Neuquén: evidencia de volcanismo jurásico en la Cuenca Neuquina. *Rev. Asoc. Geol. Argent.* 60 (3), 552–558.
- Llambías, E.J., Palacio, M., Danderfer, J.C., Brogioni, N., 1978. Petrología de las rocas ígneas Cenozoicas del Volcán Domuyo y áreas adyacentes. VII Congreso Geológico Argentino, Neuquén, Argentina, Actas II, pp. 553–568.
- Lorant, F., Prinzhofer, A., Behar, F., Huc, A.Y., 1998. Carbon isotopic and molecular constraints on the formation and the expulsion of thermogenic hydrocarbon gases. *Chem. Geol.* 147, 249–264.
- Mamyrin, B., Tolstikhin, I., 1984. Helium isotopes in nature. In: Fyfe, W. (Ed.), *Development in Geochemistry*. Elsevier, Amsterdam, p. 288.
- Marty, B., Jambon, A., 1987. C³He in volatile fluxes from the solid Earth. Implications for Carbon geodynamics. *Earth Planet. Sci. Lett.* 83, 16–26.
- Marty, B., Zimmermann, L., 1999. Volatiles (He, C, N, Ar) in mid-oceanic ridge basalts: assessment of shallow-level fractionation and characterization of source composition. *Geochim. Cosmochim. Acta* 63, 3619–3633.
- Mas, L.C., Mas, G.R., 2015. Geothermal energy development at Copahue volcano. In: Tassi, F., Vaselli, O., Caselli, A. (Eds.), *Copahue Volcano Active Volcanoes of the World Book Series*. Springer-Verlag, Berlin Heidelberg, pp. 257–271.
- Mas, G.R., Bengochea, L., Mas, L.C., Lopez, N., 2009. Hydrothermal explosion due to seal effect in el Humazo geothermal manifestation, Domuyo volcano, Neuquén, Argentina. 34th Workshop on Geothermal Reservoir Engineering Stanford University, Stanford, California, p. 5.
- Miranda, F., Folguera, A., Leal, P.R., Naranjo, J.A., Pesce, A., 2006. Upper Pliocene to Lower Pleistocene volcanic complexes and Upper Neogene deformation in the south-central Andes (36°30'–38°S). *Geol. Soc. Am. Special Paper* 407 .
- Montegrossi, G., Tassi, F., Vaselli, O., Bucciati, A., Garofalo, K., 2001. Sulfur species in volcanic gases. *Anal. Chem.* 73, 3709–3715.
- Ozima, M., Posodek, F.A., 1983. *Noble Gas Geochemistry*. Cambridge University Press, Cambridge .
- Palacio, M., Llambías, E.J., 1978. Las Fuentes termales del volcán domuyo, Provincia del Neuquén. VII Congreso Geológico Argentino, Neuquén, Argentina, Actas, II, pp. 145–159.
- Palma, R.M., Kietzmann, D.A., Martín-Chivelet, J., López-Gómez, J., Bressan, G.S., 2012. New biostratigraphic data from the Callovian–Oxfordian La Manga Formation, Neuquén Basin, Argentina: evidence from an ammonite condensed level. *Paleobiol. Spec. Rev.* 11, 345–356.
- Pineau, F., Javoy, M., 1983. Carbon isotopes and concentration in mid-oceanic ridge basalts. *Earth Planet. Sci. Lett.* 62, 239–257.
- Poreda, R.J., Craig, H., 1989. Helium isotope ratios in circum-Pacific volcanic arcs. *Nature* 338, 473–478.
- Ramos, V.A., Cristallini, E., Introcaso, A., 2004. The Andean thrust system latitudinal variations in structural styles and orogenic shortening. In: McClay, K. (Ed.), *Thrust Tectonics and Hydrocarbon Systems*. AAPG Spec Vol. Memoir. 82, pp. 30–50.
- Rizzo, A., Barberi, F., Carapezza, M.L., Di Piazza, A., Francalanci, L., Sortino, F., D'Alessandro, W., 2015. New mafic magma refilling a quiescent volcano: evidence from He–Ne–Ar isotopes during the 2011–2012 unrest at Santorini, Greece. *Geochem. Geophys. Geosyst.* 16 (3):798–814. <http://dx.doi.org/10.1002/2014GC005653>.
- Sano, Y., Naoto, T., Nishio, Y., Fischer, T.P., Williams, S.N., 2001. Volcanic flux of nitrogen from the Earth. *Chem. Geol.* 171, 263–271.
- Snyder, G., Poreda, R., Fehn, U., Hunt, A., 2003. Sources of nitrogen and methane in Central American geothermal settings: noble gas and 129I evidence for crustal and magmatic volatile components. *Geochem. Geophys. Geosyst.* 4. <http://dx.doi.org/10.1029/2002GC000363>.
- Symonds, R.B., Gerlach, T.M., Reed, M.H., 2001. Magmatic scrubbing: implication for volcano monitoring. *J. Volcanol. Geotherm. Res.* 108, 303–341.
- Taran, Y.A., Pokrovsky, B., Esikov, A., 1989. Deuterium and oxygen-18 in fumarolic steam and amphiboles from some Kamchatka volcanoes: "andesitic waters". *Doklady Akademii Nauk SSSR.* 304, pp. 440–443.
- Tassi, F., Aguilera, F., Benavente, O., Paonita, A., Chiodini, G., Caliro, S., Agusto, M., Gutierrez, F., Capaccioni, B., Vaselli, O., Caselli, A., Saltori, O., 2016. Geochemistry of fumarolic fluids from Pteroa volcano (Argentina–Chile) in 2010–2015: insights into compositional changes related to the fluid source region(s). *Chem. Geol.* (in publ).
- Taylor, H., 1986. Magmatic volatiles: isotopic variation of C, H and S. In: Taylor, H.P., O'Neil, J.R. (Eds.), *Stable Isotopes in High Temperature Geological Processes*. *Rev. Mineral.* 16, pp. 185–225.
- Truesdell, A.H., Hulston, J.R., 1980. Isotopic evidence on environments of geothermal systems. In: Fritz, P., Fontes, J.C. (Eds.), *Handbook of Environmental Isotope Geochemistry/The Terrestrial Environment*, A 1. Elsevier, Amsterdam, pp. 179–226.
- Vaselli, O., Tassi, F., Montegrossi, G., Capaccioni, B., Giannini, L., 2006. Sampling and analysis of fumarolic gases. *Acta Vulcanol.* 18, 65–76.
- Völker, D., Kutterolf, S., Wehrmann, H., 2011. Comparative mass balance of volcanic edifices at the Southern Volcanic Zone of the Andes between 33°S and 46°S. *J. Volcanol. Geotherm. Res.* 205, 114–129.
- Whiticar, M.J., 1999. Carbon and hydrogen isotope systematics of bacterial formation and oxidation of methane. *Chem. Geol.* 161, 291–314.
- Zhu, Y., Shi, B., Fang, C., 2000. The isotopic compositions of molecular nitrogen: implications on their origins in natural gas accumulations. *Chem. Geol.* 164, 321–330.